Chemistry & Biology, Vol. 11, 1383–1394, October, 2004, ©2004 Elsevier Ltd. All rights reserved. DOI 10.1016/j.chembiol.2004.08.012

Crystal Structure and Mechanistic Implications of 1-Aminocyclopropane-1-Carboxylic Acid Oxidase—The Ethylene-Forming Enzyme

Zhihong Zhang,[1] Jing-Shang Ren,[2] Ian J. Clifton,[1] and Christopher J. Schofield[1,*]
[1]The Oxford Centre for Molecular Sciences and
The Department of Chemistry
University of Oxford
Chemistry Research Laboratory
Mansfield Road
Oxford OX1 3TA
United Kingdom
[2]The Division of Structural Biology
The Wellcome Trust Centre for Human Genetics
Roosevelt Drive
Headington, Oxford OX3 7BN
United Kingdom

Summary

The final step in the biosynthesis of the plant signaling molecule ethylene is catalyzed by 1-aminocyclopropane-1-carboxylic acid oxidase (ACCO). ACCO requires bicarbonate as an activator and catalyzes the oxidation of ACC to give ethylene, CO_2, and HCN. We report crystal structures of ACCO in apo-form (2.1 Å resolution) and complexed with Fe(II) (2.55 Å) or Co(II) (2.4 Å). The active site contains a single Fe(II) ligated by three residues (His177, Asp179, and His234), and it is relatively open compared to those of the 2-oxoglutarate oxygenases. The side chains of Arg175 and Arg244, proposed to be involved in binding bicarbonate, project away from the active site, but conformational changes may allow either or both to enter the active site. The structures will form a basis for future mechanistic and inhibition studies.

Introduction

Ethylene is produced in all higher plants and has been used since ancient times to accelerate fruit ripening. It acts as a signaling molecule (or growth "hormone") involved in the regulation of ripening in climacteric fruits, pigmentation, senescence, leaf/flower abscission, and other aspects of plant development and defense. Ripening of climacteric fruits can be induced by exposure to ethylene and is limited by its absence. Both the control of environmental ethylene and its endogenous biosynthesis are of considerable agricultural and commercial importance [1–4].

Ethylene is biosynthesized in two steps, catalyzed by ACC synthase and ACC oxidase (ACCO, the ethylene-forming enzyme), from S-adenosy-*L*-methionine (SAM) (Figure 1). Both ACC synthase and ACCO exist as multigene families, active under different physiological conditions, reflecting a requirement for regulation of the multiple roles of ethylene. ACC synthase, which is pyridoxal phosphate dependent, catalyzes the cyclization of SAM to give 5′-methylthioadenosine, which is recycled to *L*-methionine via the Yang cycle [5], and ACC. Crystal structures for ACC synthase complexed with pyridoxal-5′-phosphate have been reported and together with kinetic studies these have enabled detailed mechanistic proposals [6]. However, until recently the complex mechanism of the ACCO catalyzed reaction has remained obscure.

ACCO is a member of a superfamily of oxygenases and oxidases, most of which utilize Fe(II) as a cofactor and 2-oxoglutarate (2OG) as a cosubstrate [7]. The 2OG oxygenases are involved in many biosynthetic pathways, e.g., those leading to collagen, the β-lactam antibiotics, and modified amino acids and peptides [8, 9]. They also play a key role in the hypoxia-inducible factor signaling pathway for hypoxic sensing in mammals [10]. Sequence analyses informed by structural studies have identified many putative members of the family in plants, with ca. 100 examples being identified in the *Arabidopsis thaliana* genome. "2OG oxygenases" have a requirement for Fe(II) and catalyze a variety of two-electron oxidations including hydroxylations, desaturations, and oxidative ring closures. Along with another member of the structural family, isopenicillin *N* synthase (IPNS) (Figure 1B) [11], ACCO is unusual as it does not use 2OG as a cosubstrate. It is possible that, in addition to ACCO and IPNS, other atypical members of the family exist; the unusual epimerization reaction catalyzed by carbapenem synthase (CarC) [12, 13] may have a mechanistic relationship with ACCO.

ACCO couples the two-electron oxidation of ACC to give ethylene, CO_2, and cyanide [5, 14, 15] (Figure 1A). In vitro, catalytic oxidation of ACC can be coupled to the oxidation of ascorbate. ACCO has a complex kinetic mechanism and is prone to inactivation in vitro, undergoing fragmentation and oxidative modification. Further, it is unusual in that it requires bicarbonate as an activator [14, 16, 17]. The addition of bicarbonate to ACCO incubations both increases k_{cat} and protects ACCO from oxidative deactivation [18].

Spectroscopic and crystallographic studies have revealed that the mechanisms of ACCO, IPNS and the 2OG dependent oxygenases involve binding of dioxygen to a five-coordinate Fe(II) ion in the enzyme-substrate complex [9, 19–23]. Crystallographic analyses on IPNS-Fe(II)-substrate complexes [23] together with those of closely related 2OG oxygenases (e.g., deacetoxycephalosporin C synthase, DAOCS) [24] have enabled some of the structural elements that distinguish IPNS from its 2OG utilizing relatives to be identified. Mutagenesis studies have led to proposed roles for residues in ACCO catalysis, including the iron binding ligands, various lysyl residues possibly involved in ascorbate binding, and arginine (Arg244, using the tomato pTOM13 ACCO numbering system), serine (Ser246), and threonine (Thr157) residues in binding the ACC carboxylate or bicarbonate [25, 26]. As yet, conclusive assignments for the roles of these residues have yet to be made; kinetic analyses have been hampered by the lability of ACCO and low

*Correspondence: christopher.schofield@chem.ox.ac.uk

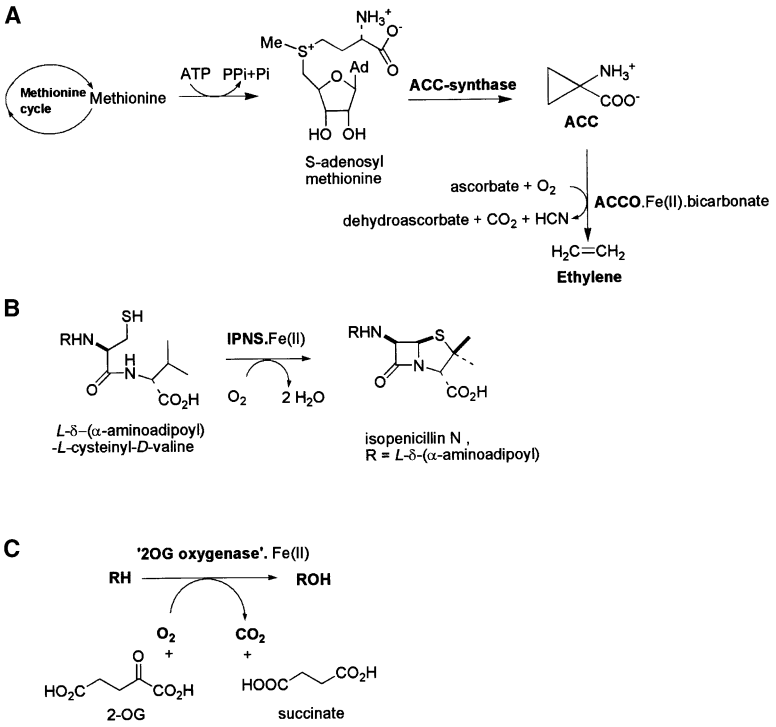

Figure 1. The ACCO Reaction and Those of Related Enzymes

(A) The biosynthesis of ethylene.

(B) The isopenicillin *N* synthase catalyzed reaction.

(C) Stoichiometry of a 2-oxoglutarate dioxygenase catalyzed hydroxylation.

levels of substrate turnover with some isoforms. We report the crystal structure of *Petunia hybrida* ACCO and discuss how it relates to current mechanistic proposals, the identity of residues involved in catalysis, and the lability of ACCO.

Results and Discussion

Crystallization and Structure Solution

After some effort employing ACCO isoforms from different sources (including tomato, kiwi and apple) with different C termini (see below), it was found that macroseeding techniques employing ACCO from *P. hybrida* provided crystals suitable for diffraction analysis. Complexes of ACCO with Fe(II) and Co(II) were obtained by soaking under anaerobic conditions. The structures were solved by molecular replacement using a model obtained by multiple-wavelength anomalous dispersion on SeMet substituted apo-ACC oxidase. Except in the region of the iron binding site (Figures 2, 3, 4A, and 4B), all three structures (apo-ACCO, ACCO-Fe(II) and ACCO-Co(II) complexes) were similar (rms deviation for the backbone atoms, 0.24 Å between apo-ACCO and ACCO-Fe(II), and 0.32 Å between apo-ACCO and ACCO-Co(II)). Soaking experiments with the metal complexes of ACCO did not lead to the clear observation of ACC complexed to the metal possibly due to interactions between different ACC monomers in the crystalline state (see below).

In the description of the ACCO structure (Figures 2–4), comparisons are made with IPNS, DAOCS and ANS (anthocyanidin synthase), three enzymes for which structures are available and which belong to the same subfamily as ACCO [11, 24, 27, 28]. ANS catalyzes the oxidation of the flavonoid C-ring in the biosynthesis of the anthocyanin class of flavonoids [27, 29]. Structural comparisons with other 2OG oxygenases are made where appropriate. Except where stated the numbering refers to the *P. hybrida* ACCO.

Monomer Structure and Topology

The main chain of the ACCO contains eleven α helices and thirteen β strands (Figure 3A). Eight (β-4 to β-11) of the β strands form the distorted double-stranded β helix (DSBH or jellyroll) core common to all members of the 2OG oxygenases for which crystal structures are available (e.g., see ref. [11, 21, 23, 24, 30]). The DSBH is also present in the cupin family of plant proteins and is characteristic of the JmjC (jumonji C) transcription factors. The sequences between residues 267 and 274 and 310 and 319, which display low similarity among ACCO isoforms and are both well away from the active site, are disordered. Most of the helical regions are located to the N-terminal (α-1 to α-6) and C-terminal (α-8 to α-11) sides of the DSBH. The N-terminal helices appear to form a supporting matrix on one face of the DSBH. The active site is located at one end of the DSBH and appears to be open compared to those for IPNS and 2-OG oxygenases [11, 24, 27]. Like DAOCS [24], ANS [27] and IPNS [11] one 'sheet' of the DSBH is extended by two β strands (β-1 and β-2, adjoining β-6 of the DSBH). The other end of the sheet of the DSBH of ACCO is extended by β-3 (adjoining β-1 of the DSBH), which is located between two conserved α helices (α-3 and α-4). The DSBH is stabilized by hydrophobic interactions that involve residues including Ile184, Leu186, Gln188, Phe187, Phe250, Val214, Val215, Leu195, Leu197, Val236, Phe33 and Val206. Many of these residues are well conserved with IPNS, DAOCS, and ANS. Indeed, despite a lack of overall sequence identity [ACCO:IPNS, ca. 16% overall identity (25.6% identical

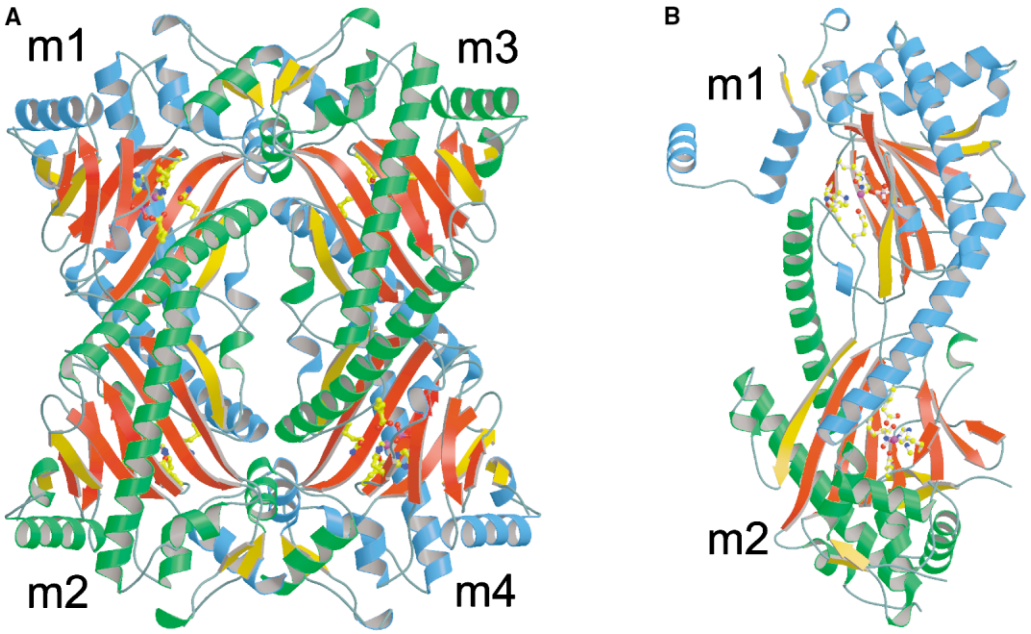

Figure 2. Views of the Crystal Structure of ACCO Showing the Tetrameric and Dimeric Forms

(A) shows tetrameric and (B) dimeric. The double-stranded helix (DSBH) cores are colored in red, non-core strands are colored in gold, and the helices are colored in green or blue for alternating monomers. Active site residues are drawn in ball and stick form. Individual ACCO monomers are assigned as m1, m2, m3 and m4.

over 203 residues); ACCO:ANS, ca. 24% identity (32% identity over 228 residues)], the conformation of the DSBH core of ACCO is remarkably similar to that of IPNS and related 2OG oxygenases (r.m.s. deviation of backbone atoms for ACCO with respect to ANS is 1.54 Å and for IPNS it is 1.49 Å) (Figure 3). However, differences in specific secondary structure elements of ACCO render it unusual. Although some of these differences may be artifacts due to the constraints of the crystalline lattice, together with mutagenesis data and mechanistic proposals, they will provide the basis for a structural explanation of the unusual properties of ACC oxidase.

The Oligomeric State and C Terminus of ACCO

In IPNS and related 2OG oxygenases the C terminus has been proposed to form a "lid" over the active site. In the IPNS crystal structure obtained without substrate, Gln330, the penultimate residue on the C terminus projects into the active site such that its side chain is close to the metal [Mn(II) substituting for Fe(II)] (Figure 4D) [11]. Upon substrate binding this residue is displaced from the immediate vicinity of the Fe(II) (Figure 4E) [23]. The catalytically active forms of IPNS, ANS, and DAOCS are thought to be monomeric, though the latter is prone to oligomerization at high concentration and in the crystalline state [31]. In comparison, other 2OG oxygenases, e.g., FIH (factor inhibiting hypoxia-inducible factor) and procollagen prolyl-4-hydroxylase, are oligomeric [32–35]. Gel filtration analyses with *P. hybrida* ACCO in 50 mM phosphate buffer (pH 7.5) detected only a monomeric form of the protein. Analyses using "native" (i.e., soft ionization) electrospray ionization mass spectrometry led to the detection of both monomeric and dimeric forms. Light scattering employing ACCO in the crystallization buffer indicated that oligomerization did occur (Z.Z. et al., unpublished data).

The C terminus of ACCO comprises β-13, a short 3_{10} helix (α-9) and two longer helices (α-10 and α-11) (Figures 2 and 3). As in IPNS and ANS, α-10 (the penultimate helix in ACCO) helps to enclose the active site and side chains of residues from its inner face project toward the active site (see below). At least in the crystal structure the final helix of ACCO points away from the DSBH/active site, leaving it open and precluding any interaction of the residues on the C terminus with the active site of the same monomer metal as observed in the IPNS-Mn(II) complex. However, in the monomeric form this helix may help to enclose the active site. The final helix present in the *P. hybrida* ACCO is apparently absent in the ANS crystal structure (although the final nine residues, 348 to 356, were disordered).

The C terminus of each ACCO monomer interlocks with the C terminus of an adjacent molecule to form a tetramer (Figure 2A). Both hydrophobic and electrostatic interactions appear to be involved at this interface involving the following residues: Glu222 (m1) to Lys297 (m3); Lys279 (m1) to Met304 (m3) via a water molecule; Leu288 (m1) to Phe294 (m3); Phe294 (m1) to Phe294 (m3); and Arg300 (m1) to Asp219 and Tyr285 (m3).

This interlocking arrangement observed between the C termini of ACCO monomers in the crystalline state is reminiscent of that which enables the catalytically active dimeric form of FIH where the dimer interface also involves an interlocking arrangement involving predominantly hydrophobic interactions between two C-terminal helices. The C-terminal monomer-monomer interactions of FIH involve a substantial buried surface area of 3210 $Å^2$. In ACCO the contacts between the C termini

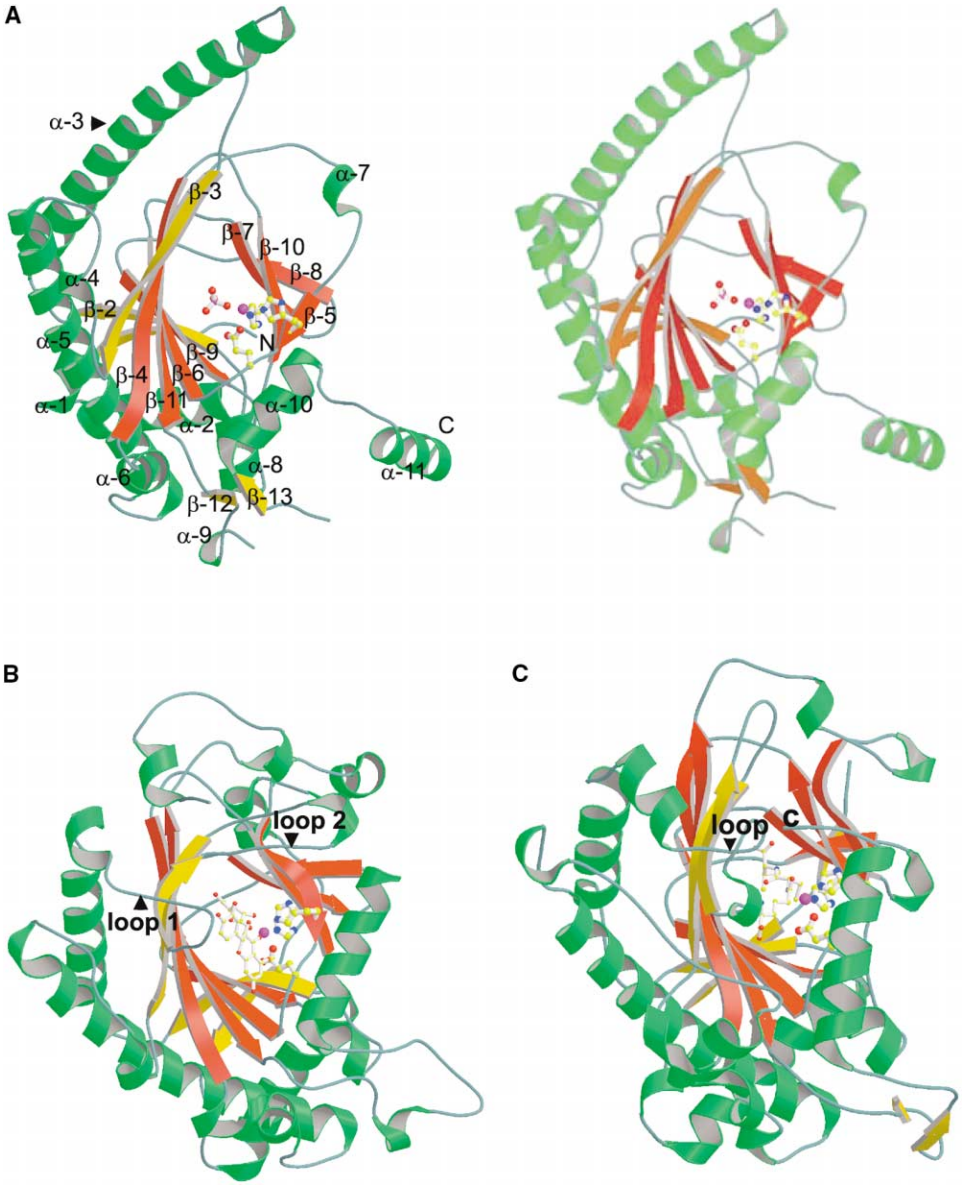

Figure 3. Overall View of the ACCO Structure and Comparison with ANS and IPNS

(A) Stereoview of ACCO showing the double-stranded β-helix (DSBH) topology and the location of Fe(II) (in magenta). The α helices are in green, the DSBH core strands are in red, and non-core β strands are in gold. The side chains of Fe(II) binding residues (His177, Asp179, His234) and the ligating phosphate or sulfate are in ball and stick form. The extended helix α-3 is arrowed.

(B) View of the structure of ANS (PDB 1GP5) complexed with Fe(II), 2OG, and dihydroquercetin. Two loops that help to enclose the ANS active site, making it more enclosed than that of ACCO in the crystalline form, are labeled as loops 1 and 2. The substrate and residues binding to Fe(II) atom are in ball and stick form. The color assignments for α helices and β strands are as in (A).

(C) View from the crystal structure of the IPNS-Fe(II)-ACV (PDB 1BK0) complex showing the loop (labeled) and the C terminus that forms a "lid" over the active site. All color assignments are as in (A). Note that the ACCO active site is the most open, at least in the crystalline form (see text).

of adjacent monomers appear to be weaker (surface area 2677 Å^2). Given the role of FIH in the hypoxic response and the precedent for oligomerization in regulation of signaling pathways, the similarity between FIH and ACCO in their C-terminal region is interesting. However, since FIH and ACCO belong to different structural subfamilies it may be coincidental.

Preliminary mutation studies on the C terminus of tomato ACCO pTOM13 are consistent with it playing a role in catalysis (Z.Z. and C.J.S., unpublished data). Truncation of the tomato pTOM13 ACCO C terminus after Met304 or deletion of the loop between Glu267 to Gln275 (or Glu272 to Gln275) generated mutants with significantly reduced activity of $<$5% of wild-type ACCO, i.e., ACC oxidation was proceeding at a stoichiometric or substoichiometric level. Truncation of the tomato ACCO from Glu302 led to (almost) complete ($<$1%) loss of activity. The activity of these mutants was still stimulated

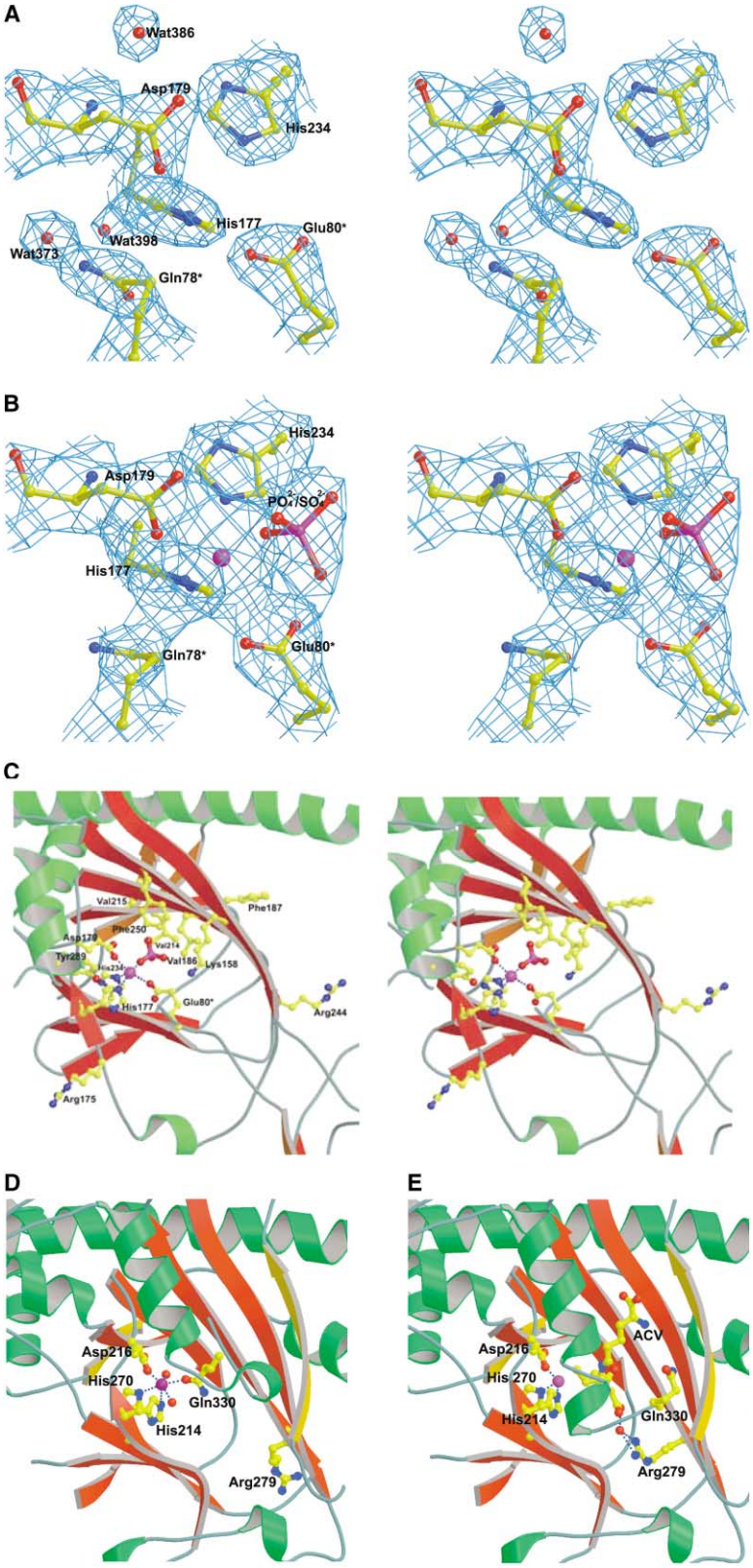

Figure 4. Close-Up View of the ACCO Active Site and Comparison with Those of IPNS in the Presence of Mn and Fe(II)

(A and B) The $2mF_o - DF_c$ electron density map, contoured at 1.0 σ, of the active site of ACCO in the absence and presence of Fe(II).

(C) Stereoview of the active site of ACCO. Fe(II) ligating residues and phosphate/sulfate ion are in ball and stick form; dotted lines indicate ligation to the iron atom from these species. Also in ball and stick form are the residues between which fragmentation has been shown to occur (Leu186/Phe187 and Val214/Val215) and the residues (Arg175 and 244) proposed to be involved in catalysis either by binding to substrate and/or bicarbonate (see text).

(D and E) The active sites of IPNS-Mn(II) (PDB 1IPS) and IPNS-Fe(II)-ACV (PDB 1BK0) complexes showing the conformational change involving Arg279. Mn is colored in dark purple and Fe(II) in magenta. An analogous conformational change may occur with Arg244/Arg175 of ACCO.

by bicarbonate. Single mutations of individual residues in the C terminus of pTOM13 ACCO, Phe301Tyr, Glu302Gln/Arg, Ala303Gly, and Met304Ile all generated proteins retaining significant activity. ACC oxidases from different sources reveal variations in the identity and number of residues at the C terminus, i.e., subsequent to α-11

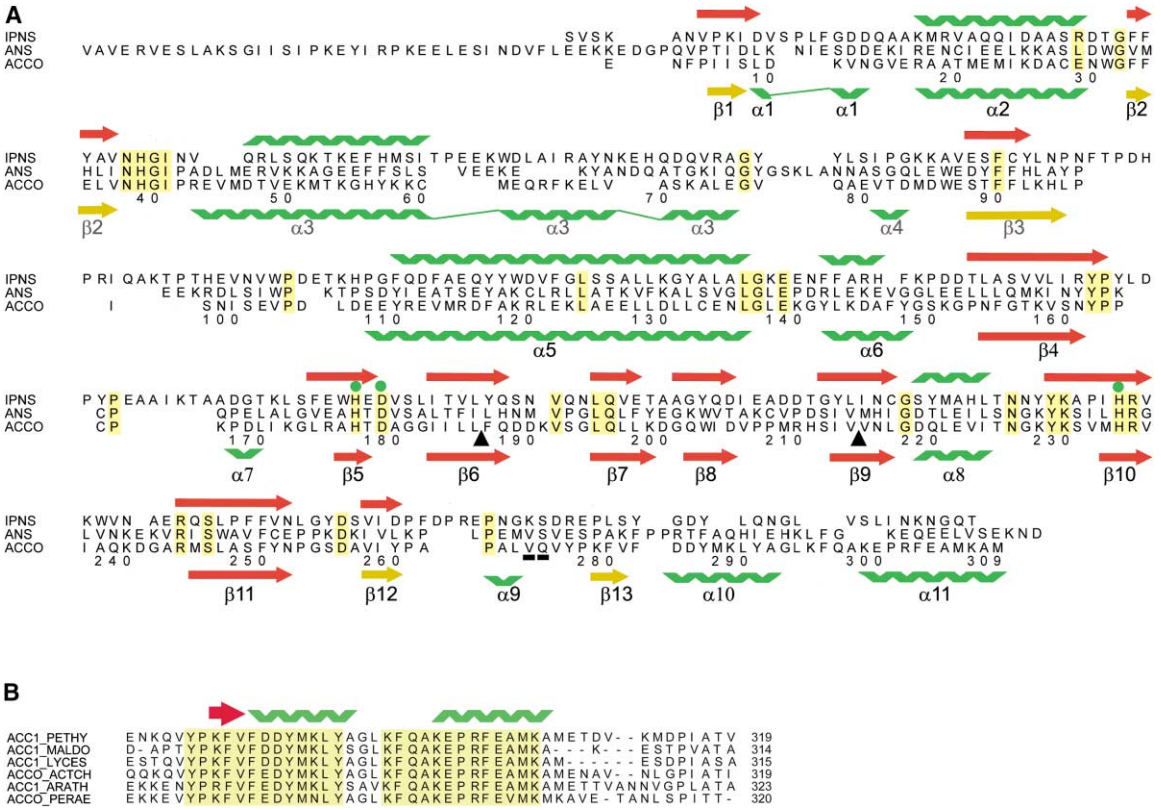

Figure 5. Sequence Comparisons Based on the Structures of ACCO

(A) Sequence comparisons based on the structures of ACCO (*P. hybrida*), IPNS (PDB 1BK0) and ANS (PDB 1GP6). The secondary structures shown above the sequences are conserved. Those shown below the sequences are as assigned for ACCO. Helices are in green, non-DSBH core strands are in gold and the DSBH core strands are in red. The Fe(II) ligating residues are indicated with green dots; "autocleavage" sites are marked with triangles and residues conserved throughout the 3 enzymes are highlighted in yellow. The ACCO sequences between the two underlined residues, 266 and 275, and after residue 309 are omitted.

(B) Sequence comparisons of the C termini of different ACCOs; secondary structure assignment is based on the structure of *P. hybrida* ACCO. Identical sequences are highlighted in yellow. Shown are sequences of ACC1-PETHY from *P. hybrida* (SWISSPROT Q08506), ACC1_MALDO from apple (SWISSPROT Q0985), ACC1_LYCES from tomato (SWISSPROT P-5116), ACCO_ACTCH from kiwi (SWISSPROT P31237), ACC1_ARATH from *Arabidopsis thaliana* (SWISSPROT Q06588), and ACCO_PERAE from avocado (SWISSPROT P19464).

of the *P. hybrida* enzyme (Figure 5B). The C terminus of ACCO may play a role in effecting completion of catalytic cycles via assisting in the reduction of an oxidized form of the enzyme after oxidation of ACC (see below) [18]. The use of ACC oxidases with significantly different C termini may also account, at least in part, for discrepancies in the order of substrate binding arising from kinetic analyses using different ACC oxidases [36, 37].

The Presence of an Extended Helix

The most striking difference between the ACCO structure and those of related enzymes concerns α-3 (residues 43 to 75), which is considerably extended in ACCO (Figure 3A). In ACCO, together with its accompanying strand (β-3) and turn, α-3 forms a "proboscis" that projects about 25-30 Å from the surface of each monomer. An analogous helix to α-3 is present in all 2OG oxygenases (and IPNS) that have been structurally characterized, but is typically longer in the IPNS/DAOCS/ANS subfamily than some other subfamilies (e.g., the "CAS" subfamily). In ACCO the unusually long α-3 is stabilized by intramolecular hydrophobic interactions between α-3 and its accompanying strand (β-3), including those involving the side chains of Leu68 with those of Ala79 and Met84, and the electrostatic interactions between Arg64 and Asp85, and Tyr57 and Trp86.

In the crystalline lattice the side chains of Gln78, Glu80, and Asp83, located on a loop just past the end of α-3, project into the active site of a symmetry related ACCO monomer (Figure 2A). The side chains of these residues are in position to form interactions with residues in the adjacent monomer including Gln78 (m1) to His177 and Tyr289 (m2), Asp83 (m1) to Lys158 (m2), and Glu80 (m1) to the Fe(II) of m2. The distance from the side chain carboxylate of Glu80 (m1) to the Fe(II) (m2) is 2.9 Å. These interactions are important not least because Glu80 is involved in binding the iron and Lys158 and Tyr289 may be involved in catalysis (see below).

The Active Site

On the inner face of the active site the residues are mostly hydrophobic and well conserved as identical or similar residues compared to IPNS/ANS (Figure 4) [23, 27]. However, the active site of ACCO is relatively open

in the crystal form (Figure 3A). Structural reasons for the open nature of the ACCO active site compared to those of IPNS and ANS include the following: (1) the presence of the extended α-3 contributes to the open nature of the active site. In ANS [27] two large loops (residues 127–139 and residues 114–123) border one face of the active site helping to enclose it (Figure 3B). In IPNS [23] one of these loops is orientated further away from the active site than in ANS, but this loss of "cover" is apparently compensated for by inward movement of its C-terminal α-helix (α-10) and the presence of another loop from the N-terminal region (110–126) (Figure 3C). Due to the extended nature of α-3 of ACCO, neither of these two loops can be involved in enclosing its active site; (2) the conformation of a loop in ANS/IPNS (residues 127–139 in ANS) projects the side chains of residues Asn115, Gln117, and Ile122 toward the active site. However in ACCO the conformation of the analogous loop (residues Val69 to Gly76) is such that the side chains of its residues do not project toward the active site; (3) the final α-helix (α-11) of ACCO is directed away from the active site rather than toward it as in, e.g., IPNS; and (4) ACCO lacks the N-terminal arrangement of three helices present in ANS and predicted to be present in some other plant 2OG oxygenases including FLS (flavonol synthase), giberellin 3β-hydroxylase and FHT (flavanone 3β-hydroxylase) [27].

Coordination Chemistry

The ACCO-Fe(II) and ACCO-Co(II) structures reveal the metal ligated by the side chains of His177, Asp179, and His234 (Figures 4B and 4C). The conformations of the side chains of the "facial triad" of iron ligands in ACCO are similar to those in related enzymes (Figures 3, 4, and 6) [38]. The observation of Co(II) binding in the same position as Fe(II) is interesting as Co(II) has been used to inhibit ethylene biosynthesis. The structures confirm the assignment of the identity of the facial triad of residues as the Fe(II) binding ligands as assigned by mutagenesis studies [39] and reveal that the positions of other point mutants of conserved histidinyl residues (H39Q, H56Q and H94Q, H211Q) are consistent with their retention of catalytic activity [40]. The refined metal-ligand distances are 2.5 Å for His177, 2.4 Å for Asp179, and 2.2 Å for His234. Asp179 is in position to ligate the metal via a single carboxylate oxygen. In the ACCO-Fe(II) and ACCO-Co(II) structures, a phosphate ion from the crystallization buffer (the possibility that the ion is a sulfate cannot be ruled out), was observed in position to ligate to the metal (shortest P-O to Fe distance is 2.1 Å). Glu80 of another ACCO monomer, located on the loop between the "extended helix" α-3 and β-3, also approaches the metal (O to Fe distance: 2.9 Å) (Figures 2B and 4A). The side chain of Phe250, which is conserved in IPNS and ANS, points directly at the iron (C-4 of phenyl ring to Fe: 5.8 Å). The presence of Asn252 close to the metal is notable since it is conserved in IPNS but not ANS (where it is a Glu residue) [23, 27]. This residue probably serves to stabilize the iron binding site and may be involved in dioxygen binding. The side chains of two tyrosines, Tyr289 and Tyr285, located on α-10, also point toward the metal; the distances of their phenolic oxygen to the Fe(II) are 7.9 Å and 12.5 Å, respectively. These distances may decrease if conformational changes allow α-10 to approach the active center. Tyr289, in particular, could be involved in mediating electron transfer to the metal center (see below).

Possible Role of Conserved Residues in Bicarbonate and Substrate Binding

Mutagenesis studies have aimed to identify the residues involved in bicarbonate, ACC, and ascorbate binding during ACCO catalysis [25, 26], but have not conclusively identified the residues involved in the binding substrate/bicarbonate. However, the mutagenesis work on conserved lysyl residues led to the observation that substitution of Lys158 of kiwi fruit ACCO results in a large reduction in activity, but that stimulation by bicarbonate still occurred [26]. In the crystal structures, the side chain of Lys158 projects directly into the ACCO active site and adopts a similar conformation to that observed for the analogous conserved lysine in ANS (Lys213), where it is probably involved in substrate binding [27]. The distance from the amine group of Lys158 of ACCO to the metal ion is 7.9 Å. The Lys158 side chain is also close to that of Asp83 from another ACCO monomer—thus in the monomeric form of ACCO in solution the side chain of Lys158 may be "free" to approach the iron at a closer distance.

Kinetic analyses on ACCO have revealed that mutation of the residue adjacent to Lys158, Thr157, affects both the K_m of ACC and V_{max} [25]. The structures suggest that Thr157 is unlikely to be directly involved in binding ACC and it is not conserved. Thus, the effect of mutation of Thr157 may be due to perturbation of Lys158. ACCO is competitively inhibited with respect to ascorbate by pyridoxal phosphate [25]. Lys158 should be accessible for Schiff base formation with pyridoxal phosphate. Since there appears to be space in the region of the active site adjacent to Lys158, derivatives of ascorbate modified on its side chain (e.g., 5,6-isopropylidene *L*-ascorbate), which can substitute efficiently for ascorbate itself, could also be accommodated in this region. It is also possible that Lys158 is involved in binding ACC (either prior to or, less likely, during ACC ligation to iron).

The RXS Motif and Arg175

Arg244 and Ser246 form an RXS motif, which together with Tyr162 is conserved in the structural subfamily to which ACCO belongs. These residues bind the 5-carboxylate oxygen of 2OG in ANS and DAOCS and, in IPNS, bind one carboxylate of the tripeptide substrate [23]. In ACCOs the RXS motif is entirely conserved and is proposed to be involved in binding the carboxylate of ACC. In contrast to the ANS and the IPNS substrate complex structures, the side chain of Arg244 of ACCO is directed away from the active site and is in position to form an electrostatic interaction with a sulfate ion on the exterior of the protein (Figure 4C). The position of the sulphate may reflect bicarbonate binding; however, given the importance of bicarbonate in catalysis and the distance of the sulfate/phosphate from the metal, this seems unlikely. The structure of IPNS complexed with

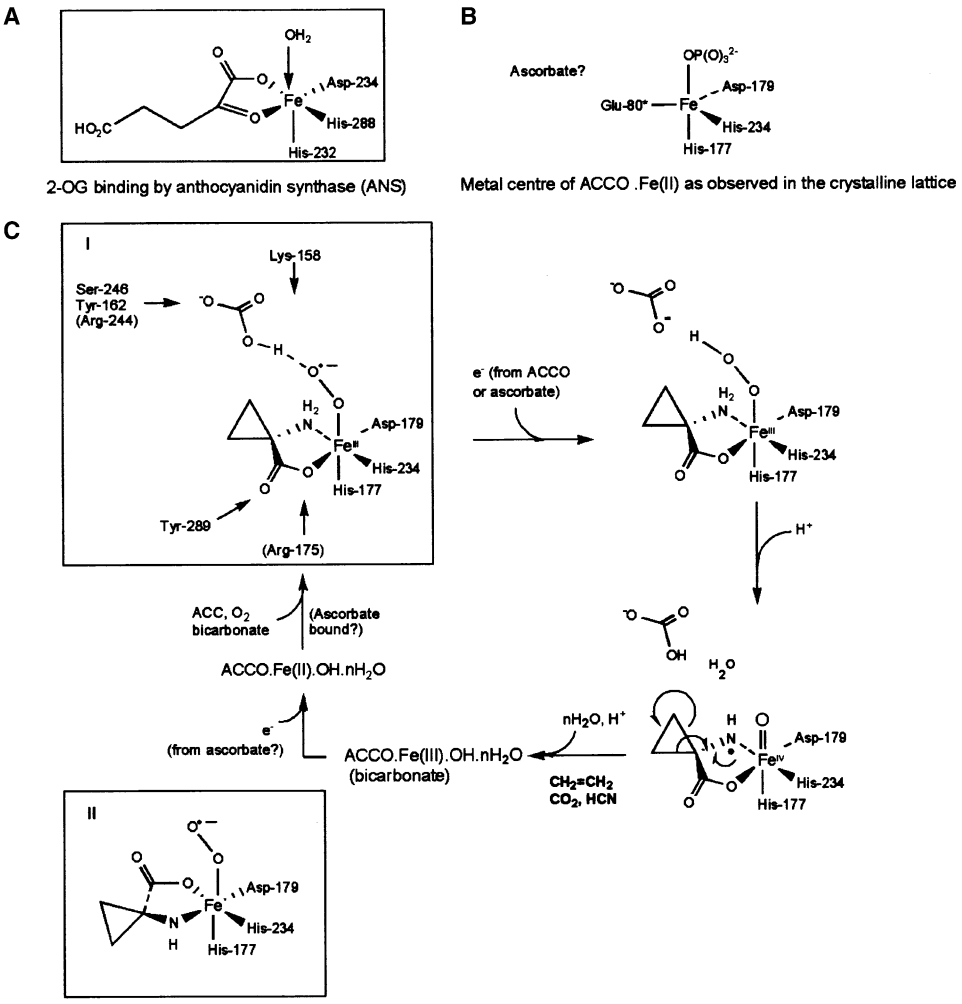

Figure 6. The Iron Binding Site of ACCO

(A) 2-OG binding at the active site Fe(II) of ANS.

(B) Metal center of ACCO-Fe(II) as observed in the crystalline lattice.

(C) Outline mechanism for ACCO following from the proposals of Rocklin et al. [26] showing a possible binding mode for ACC and binding roles of the side chains of residues discussed in the text. Other binding modes, including II, are possible. Note the side chains of Arg244 and Arg175 will have to undergo significant conformational changes to bind ACC and/or bicarbonate (see text). The redox and charge state of ascorbate and derivatives derived from it are unspecified.

Mn(II), substituting for Fe(II), reveals that, in contrast to the IPNS-Fe(II)-substrate structures, the side chain of the analogous residue to Arg244 of ACCO, Arg279, is similarly directed away from the active site (Figure 4D). Upon substrate binding, Arg279 of IPNS rotates about its C_α-C_β bond such that the side chain projects into the active site and binds the carboxylate of the valine of the substrate via a water molecule (Figure 4E). In ACCO, the peptide backbone of Arg244 and the residues immediately after it (β-11) adopt a similar conformation to those in IPNS/ANS. The backbone of the residues on the loop immediately preceding Arg244 adopts a different conformation to those observed in ANS and IPNS. Nonetheless, although it appears from the crystal structure that ACCO may require a larger conformational change than that occurring with IPNS, it is possible that upon, or concomitant with ACC and/or bicarbonate binding (see below), the side chain of Arg244 of ACCO rotates into the active site to adopt a similar conformation to those in IPNS/ANS. This movement may involve changes in the side chain conformation of Tyr162, which adopts a different conformation to that seen in the IPNS/ANS structures.

Even if the side chain of Arg244 rotates into the active site, assuming ACC is bound to the iron, it is unlikely to be close enough to directly bind the ACC carboxylate (arginine N-ϵ to Fe: ca. 21.1 Å). It may be that Arg244 is involved in indirect binding of ACC via a water molecule(s), but other possibilities seem more likely. In a scheme aimed at reconciling most of the data on ACCO, Rocklin et al. [18] propose that Arg244 binds bicarbonate, which in turn binds an iron bound dioxygen derived intermediate to enable "correct" proton and electron transfer (see below). Providing that the conformation of Arg244 can change as outlined, the ACCO structure is consistent with this proposal. Mutation of Arg244 to lysine in tomato pTOM13 ACCO caused the enzyme to

require 5-fold more bicarbonate than the wild-type for optimal activity (ca. 50 mM versus 10 mM), and the activity of the R244K mutant was increased 17-fold in the presence of 50 mM bicarbonate relative to that without added bicarbonate (Z.Z. and C.J.S., unpublished data).

Dilley et al. [25] propose that another conserved arginine in ACCO, Arg175, located on a loop the side chains of which are directed away from the active site, binds bicarbonate (Figure 4C). Mutation of Arg175, to e.g., Lys or Glu residues, resulted in a significant increase of K_a for bicarbonate. As for Arg244 it is possible to envisage a conformational change that brings the side chain of Arg175 into the active site. A conformational change involving this loop such that it adopts a similar conformation as observed in IPNS/ANS would allow the side chain of Arg175 to project toward the iron binding site. Since Arg175 is closer (N-ϵ to Fe(II) ca. 14.7 Å) to the iron than Arg244, it is possible to envisage it binding, directly or indirectly, to an iron bound ACC complex.

It is also possible that both Arg175 and Arg244 are involved in binding an ACCO-Fe-ACC-O_2-bicarbonate complex. The putative conformational changes involving Arg175 and Arg244 would render the active site of the enzyme-cofactors-substrates complex more enclosed than the open form observed in the crystal structure which may reflect a substrate capture conformation.

Inactivation of ACCO

In the absence of bicarbonate ACCO undergoes rapid inactivation. The observation that in the absence of bicarbonate ACCO is unable to efficiently oxidize ACC to ethylene but is oxidized to the ferric state [18] may reflect "incorrect" binding of ACC and/or dioxygen. ACCO also undergoes metal catalyzed autocleavage. Although not a major inactivation process under catalytic conditions for ACCO, evidence was obtained for backbone cleavage at several sites [40]. Inactivating oxidative active site modification of 2OG oxygenases is also known, including a tyrosine residue at the active site of taurine dioxygenase TauD [41, 42] and a tryptophan residue at that of AlkB [43]. N-terminal sequencing identified two cleavage sites in ACCO: one between Leu186 and Phe187, and the other between Val214 and Val215 (Figure 4C). These sites are on adjacent strands, i.e., the third (β-6) and sixth (β-9) strands of the DSBH, and are consistent with cleavage being mediated by leakage of an oxygen-derived species from the iron and specifically from the position *trans* to His177, i.e., the position occupied by the phosphate in the ACCO-Fe(II) and ACCO-Co(II) structures. The distances of the cleavage sites from the iron are such that it is unlikely that an iron bound species directly effects cleavage (the backbone N of Phe187 to the iron: 11.5 Å; the backbone N of Val215 to the iron: 11.0 Å; the carbonyl C of Val214 to Fe(II): 10.7 Å; the carbonyl C of Leu186 to Fe(II): 11.0 Å). The orientations of the cleaved amides are such that nucleophilic attack by a reactive species/α-effect nucleophile such as superoxide/peroxide that leaks from the metal may effect cleavage (or deprotonate a water to effect cleavage). Cleavage via abstraction of a C-α hydrogen of the residue on the N-terminal side of the cleaved peptide bond followed by β-scission is also possible [44], particularly for cleavage between Leu186 and Phe187, as in this case the α-H of Leu186 projects toward the metal.

Catalytic Mechanism of ACCO

In the proposals of Rocklin et al. [18, 19] for the ACCO mechanism, ACC binds to Fe(II) in a bidentate manner via its amino acid. Binding of ACC to Fe(II) may occur such that its amine is opposite to His-234 and its carboxylate group opposite to Asp179 (although the reverse is possible). This mode of binding is consistent with substrate analog studies. The observation that the 1*R*, 2*S* stereoisomer of 2-ethyl ACC is the preferred substrate of possible 2-ethyl ACC stereoisomers [45–47] is accommodated since the ethyl group will project toward a hydrophobic pocket (formed by the side chains of residues including Phe91, Phe251, and methylenes of Lys158).

Spectroscopic analyses reveal that binding of the ACC to the Fe(II) of ACCO serves to activate the enzyme for dioxygen binding by converting it from 6- to 5- coordinate [18–20]. Binding of dioxygen *trans* to His177 is consistent with the proposed roles for Arg175 and Arg244 in binding bicarbonate and/or substrate (assuming conformational changes are allowed) and the observed metal catalyzed cleavage sites. Since the ACCO-Fe-ACC-bicarbonate-dioxygen complex appears to be insufficiently reactive to effect ACC oxidation, Rocklin et al. [18] propose that initial electron transfer to the iron bound dioxygen, from ascorbate (see below) or another ACC molecule, may occur. Subsequent O-O fission, enabled by bicarbonate, can yield an iron-oxo species that effects ACC oxidation yielding ethylene, water, HCN, and ACCO-Fe(III). The latter can then be reduced by ascorbate to give ACCO-Fe(II), which is ready for another catalytic cycle (Figure 6).

If electron transfer from one ACCO monomer to another as considered by Rocklin et al. occurs [18], the observation that the loop at the end of α-3 projects into the active site of another monomer in the crystal structure may be relevant. If intramolecular electron transfer involving a protein residue occurs, Tyr289 presents itself as candidate. In the case of TauD, a tyrosine residue (Tyr73) has shown to be modified to give catechol in an inactivation process in which the new oxygen atom derives from solvent [48]. Tyr-289 of ACCO comes from a different part of the overall structure to Tyr73 of TauD, but these two enzymes come from different structural subfamilies (Tyr73 of TauD is located on an extended insert, absent in ACCO, located between the fourth and fifth strands of the DSBH).

In addition to its role as a reducing agent, possibly at two separate points in catalysis, Rocklin et al. [18] have provided evidence that ascorbate acts as an "effector" (or activator), i.e., stimulates catalysis independent of its redox properties—perhaps by helping to form a productive enzyme-substrate complex (as may occur for ANS) [27]. Although Lys158 may be involved in ascorbate binding, neither the current ACCO structure nor those for other 2OG oxygenases have identified a well-defined binding site. Nor is the stoichiometry of ACCO mediated ascorbate consumption certain. It may be that

ascorbate does not need to chelate to the metal in order to effect electron transfer (in the crystal structures of ascorbate peroxidase, ascorbate does not directly bind to the heme iron); or that electron transfer from ascorbate is mediated via specific active site residues (e.g., Tyr-289) [49].

Significance

ACCO catalyzes the final step in the biosynthesis of the plant signaling molecule ethylene that is involved in the regulation of an array of biological processes in plants, including germination, senescence, and fruit ripening. Modulation of ethylene biosynthesis is useful for control of these processes. The catalytic mechanism of ACCO is possibly the most challenging of all the non-heme iron oxygenases yet identified. Its crystal structure will provide a basis for systematic mutagenesis studies aimed at defining the role of the active site residues in binding ACC, bicarbonate, ascorbate, and dioxygen, as well as acting as template for the design of small molecule inhibitors aimed at the control of fruit ripening and other aspects of plant development.

Experimental Procedures

Expression of ACC Oxidase

The plasmid pICl0143 containing an ACCO gene (TREMBL; Q08506) from *Petunia hybrida* was donated by Dr. P. Thomas of Zeneca Agrochemicals (Jeallotts Hill Research Station, Bracknell, RG12 6EY, United Kingdom). The ACCO sequence identity was confirmed by DNA sequencing. The plasmid was transformed into *E. coli* BL21(DE3) and expression optimized. In the preparative procedure, *E. coli* BL21(DE3)/pICl0143 was grown in shake flasks (250 rpm, 27°C) containing 2× TY media supplemented with 15 μg/ml of tetracycline to late exponential phase (A_{600} ca. 0.8). ACCO production was induced by the addition of isopropyl-β-*D*-thiogalactopyranoside (IPTG) to a final concentration of 0.4 mM. Cells were grown for a further 2 hr and then harvested. Cell paste was stored at −80°C. Growth conditions for fermentation were essentially the same as for shake flask growth, except that culture growth was initiated at 37°C. When the density of the culture reached OD_{600} of ca. 1.2, the temperature was dropped to 27°C. The culture was grown at 27°C for 30 min, after which protein production was induced by IPTG. Seleno-*DL*-methionine (SeMet) substituted ACCO was produced using a metabolic inhibition protocol and LeMaster media supplemented with 50 mg/liter *DL*-SeMet. SeMet incorporation was > 90% by electrospray ionization mass spectrometric analysis.

Protein Purification

Thawed cell pellets were suspended in buffer containing 50 mM Tris-HCl (pH 7.5 at 25°C), 10% glycerol and 1 mM DTT plus 10 mM $MgCl_2$, 20 μg/ml DNase I, and a proteinase inhibitors cocktail (Sigma). The cell suspension was sonicated (5 × 20 s with 1 min cooling intervals). Polyamine (pH 8.0) was added to the resultant lysate (0.05% final concentration). Unbroken cells, cell debris and precipitated nucleic acids were then removed by centrifugation at 25,000 rpm (Beckman JA25.50, 75,600 × g) at 4°C for 30 min. The resultant supernatant was loaded onto a prepacked DEAE ion exchange (high-performance resin) column equilibrated with buffer A (25 mM HEPES-NaOH, 1 mM DTT, 3 mM EDTA, 0.5 mM benzamidine, and 10% glycerol [pH 7.5] at 25°C). After completion of sample loading, the column was washed with 2 column volumes of buffer A and bound proteins were eluted with buffer B (buffer A plus 1 M NaCl) using a linear gradient (0% to 20% B). Fractions containing ACCO (by SDS-PAGE analysis) were pooled, concentrated using an Amicon concentrator (WR Grace and Co., Danvers, MA), and loaded onto a Superdex-75 gel-filtration column equilibrated with buffer A. Proteins were eluted from the column using buffer A, and fractions containing ACCO were pooled and then loaded onto a Mono Q column equilibrated with buffer C (25 mM Tris-HCl, 1 mM DTT, and 3 mM EDTA [pH 8.0] at 25°C). Bound proteins were eluted with buffer D (buffer C plus 1 M NaCl) using a linear gradient (0%–20% D). Fractions containing ACCO were pooled and concentrated as above to ca. 35 mg/ml and stored at −80°C.

Crystallization

Initial aerobic crystallization trials with apo-ACCO employed the hanging drop vapor diffusion method at room temperature (18°C) and sparse-matrix screens from Emerald BioStructures and Hampton Research. After 10 days small rectangular crystals of recombinant *P. hybrida* ACCO were obtained from 1.2 M NaH_2PO_4, 0.6 M K_2HPO_4 and 0.3 M Li_2SO_4 buffered with 0.1 M CAPS (stock solution pH 10.5 at room temperature). These conditions were optimized to 1.05 M NaH_2PO_4, 0.5 M K_2HPO_4, 0.1 M CAPS (pH 10.3), and 0.3 M Li_2SO_4. Macroseeding was used to obtain crystals suitable for diffraction. Drops were prepared by mixing of equal volumes of protein (25 mg/ml) and well solution to a total volume of 4 μl. After 8 hr equilibration of the drop against 500 μl of well solution, macroseeds were added to the drop. Rapid formation of ingot-shaped single crystals was observed. After a week the dimensions of the crystals were ca. 0.5 × 0.2 × 0.2 mm and they were shown to belong to space group I222 with unit cell dimensions of a = 77.5 Å, b = 107.6 Å, c = 108.3 Å (apo-ACCO). Crystals of ACCO complexed with Fe(II) or Co(II) were obtained by soaking apo-ACCO crystals under anaerobic conditions in a Belle Laboratories glove box [21, 23]. Cocrystallization of ACCO with substrates and metals has not yet led to diffraction quality crystals. Apo-ACCO crystals were grown anaerobically or aerobically using the macroseeding method as above. The crystallization solution was degassed and purged with oxygen-free nitrogen gas and placed into the glove box. Fe_2SO_4 or $CoCl_2$ were dissolved in the crystallization solutions; the concentra-

Table 1. Data Collection, Phasing, and Refinement Statistics

Data Set	Se-Met Peak	Se-Met Remote	Complex with Co^{2+}	Complex with Fe^{2+}
Wavelength (Å)	0.97875	0.8856	0.8856	1.54
Cell (a, b, c) Å	70.256, 107.844, 108.046	70.298, 107.929, 108.084	70.33, 107.20, 108.41	70.34, 107.06, 108.38
Resolution (Å) (outer shell)	2.35 (2.43–2.35)	2.12 (2.2–2.12)	2.4 (2.49–2.4)	2.55 (2.69–2.55)
Measured reflection	137,404	212,171	59,817	107688
Unique reflection	17,510	23,601	16,228	12,798
Rmerge (%)	6.1	5.1	4.5	5.3
Completeness (%) (outer shell)	99.4 (96.5)	98.4 (85.8)	99.1 (99.1)	94.3 (93.4)
I/σ (outer shell)	43.6(3.75)	35.6 (1.82)	14.3 (1.3)	12.6 (1.9)
Overall figure of merit		0.649/0.4		
Refinement				
$R_{working}/R_{free}$		22.3/29.1	21.7/27.4	22.33/24.79
Rmsd from ideal geometry				
Bonds (Å)		0.0073	0.0063	0.00679
Angle (°)		1.35	1.35	1.43

tions of the metals in the drop were 5 mM. After 24 hr the crystals were frozen in the glove box and then stored in liquid nitrogen.

Data Collection

Frozen crystals were analyzed in house using CuKα radiation from a Rigaku rotating anode X-ray generator with a Mar345 detector. Cryo-protection was achieved by transferring crystals into the crystallization solution with the addition of 15% glycerol for 3 min followed by freezing in liquid nitrogen or in a liquid nitrogen stream. Apo-ACCO crystals diffracted to resolution of ca. 2.3 Å in house. The resolution obtained varied between 2.1 Å and 2.8 Å depending on the age of the crystal and/or the enzyme. Three-wavelength multiple anomalous dispersion data sets for SeMet ACCO and ACCO-Co(II) complexes were collected to 2.1 Å, and 2.4 Å resolution on Beamline 14.4, using a Mar-CCD detector, at the ESRF, Grenoble, France. Data for the ACCO-Fe(II) complex were collected in house using CuKα radiation and a Rigaku rotating anode X-ray generator with a Mar345 detector. Data were processed using Denzo, Scalepack, and the CCP4 program suite. Out of 15 methionines, including the N-terminal methionine, 13 were located and phases calculated using SHELX (Table 1). Density modification was performed using SHELX. The crystallographic asymmetric unit contained one ACCO molecule.

Model Building and Refinement

The initial model building was carried out using the automatic model building program, Arp-Warp3 [50], which led to 230 amino acid residues out of total 319 being correctly assigned. The remaining residues of the model were assigned using the program O [51]. Refinements of the model were performed using CNS [52]. One round of positional, simulated annealing and individual B factor refinement brought the R_{work} to 26.36% and R_{free} to 33.27%. 5% of the reflections were assigned for the calculation of R_{free}. The model was then adjusted and subjected to further rounds of minimization and individual B factor refinements including the addition of solvent water molecules. The final model comprised residues 2 to 266 and 275 to 309. Electron density for the residues from 267 to 274 and from 310 to 319 was unclear. In total the model contains 2372 nonhydrogen protein atoms out of a theoretical maximum of 2530. There were no outliers in the Ramanchandran plot (90.3%, 8.9% and 0.8% in the allowed, additionally allowed, and generously allowed regions, respectively). Statistics are shown in Table 1.

Acknowledgments

We thank Drs. M. McDonnough and J.M. Elkins for assistance with data collection and computing; R. Welford for reading the manuscript and useful discussions; the staff at ESRF Grenoble and SRS Daresbury for support, especially M. Walsh for his help with MAD data collection; and the BBSRC for financial support.

Received: June 2, 2004
Revised: July 15, 2004
Accepted: August 2, 2004
Published: October 15, 2004

References

1. John, P. (1997). Ethylene biosynthesis: the role of 1-aminocyclopropane-1-carboxylate (ACC) oxidase, and its possible evolutionary origin. Physiol. Plant. *100*, 583–592.
2. Pirrung, M.C. (1999). Ethylene biosynthesis from 1-aminocyclopropanecarboxylic acid. Acc. Chem. Res. *32*, 711–718.
3. Bleecker, A.B., and Kende, H. (2000). Ethylene: a gaseous signal molecule in plants. Annu. Rev. Cell Dev. Biol. *16*, 1–18.
4. Adam, D.O., and Yang, S.F. (1981). Ethylene the gaseous plant hormone—mechanism and regulation of biosysnthesis. Trends Biochem. Sci. *6*, 161–164.
5. Adam, D.O., and Yang, S.F. (1979). Ethylene biosynthesis: identification of ACC as an intermediate in the conversion of methionine to ethylene. Proc. Natl. Acad. Sci. USA *76*, 170–174.
6. Capitani, G., Hohenester, E., Feng, L., Storici, P., Kirsch, J.F., and Jansonius, J.N. (1999). Structure of 1-aminocyclopropane-1-carboxylate synthase, a key enzyme in the biosynthesis of plant hormone ethylene. J. Mol. Biol. *294*, 749–756.
7. Hamilton, A.J., Lycett, G.W., and Grierson, D. (1990). Antisense gene that inhibits synthesis of the hormone ethylene in transgenic plants. Nature *346*, 284–287.
8. Schofield, C.J., and Zhang, Z.H. (1999). Structural and mechanistic studies on 2-oxoglutarate-dependent oxygenases and related enzymes. Curr. Opin. Struct. Biol. *9*, 722–731.
9. Costas, M., Mehn, M.P., Jensen, M.P., and Que, L., Jr. (2004). Dioxygen activation at mononuclear nonheme iron active site: enzymes, models and intermediates. Chem. Rev. *104*, 939–986.
10. Schofield, C.J., and Ratcliffe, P.J. (2004). Oxygen sensing by HIF hydroxylases. Nat. Rev. Mol. Cell Biol. *5*, 343–354.
11. Roach, P.L., Clifton, I.J., Fulop, V., Harlos, K., Barton, G.J., Hajdu, J., Andersson, I., Schofield, C.J., and Baldwin, J.E. (1995). Crystal structure of isopenicillin N synthase is the first from a new structural family of enzymes. Nature *375*, 700–704.
12. Stapon, A., Li, R.-F., and Townsend, C.A. (2003). Carbapenem biosynthesis: confirmation of stereochemical assignments and the role of CarC in the ring stereoinversion process from L-Proline. J. Am. Chem. Soc. *125*, 8486–8493.
13. Clifton, I.J., Doan, L.X., Sleeman, M.C., Topf, M., Suzuki, H., Wilmouth, R.C., and Schofield, C.J. (2003). Crystal structure of carbapenem synthase (CarC). J. Biol. Chem. *278*, 20843–20850.
14. Dong, J.G., Fernandez-Maculet, J.C., and Yang, S.F. (1992). Purification and characterization of 1-aminocyclopropane-1-carboxylate oxidase from apple fruit. Proc. Natl. Acad. Sci. USA *89*, 9789–9793.
15. Peiser, G.D., Wang, T.-T., Hoffman, N.E., Yang, S.F., Liu, H.-w., and Walsh, C.T. (1984). Formation of cyanide from carbon 1 of 1-aminocyclopropane-1-carboxylic acid during its conversion to ethylene. Proc. Natl. Acad. Sci. USA *81*, 3059–3063.
16. McRae, D.G., Coker, J.A., Legge, R.L., and Thompson, J.E. (1983). CO2 requirement for ACCO. Plant Physiol. *73*, 784–790.
17. Smith, J.J., and John, P. (1993). Activation of 1-aminocyclopropane-1-carboxylate oxidase by bicarbonate/carbon dioxide. Phytochemistry *32*, 1381–1386.
18. Rocklin, A.M., Kato, K., Liu, H.-w., Que, L., Jr., and Lipscomb, J.D. (2004). Mechanistic studies of 1-aminocyclopropane-1-carboxylic acid oxidase: single turnover reaction. J. Biol. Inorg. Chem. *9*, 171–182.
19. Rocklin, A.M., Tierney, D.L., Kofman, V., Brunhuber, N.M., Hoffman, B.M., Christoffersen, R.E., Reich, N.O., Lipscomb, J.D., and Que, L., Jr. (1999). Role of the nonheme Fe(II) center in the biosynthesis of the plant hormone ethylene. Proc. Natl. Acad. Sci. USA *96*, 7905–7909.
20. Zhou, J., Rocklin, A.M., Lipscomb, J.D., Que, L., Jr., and Solomon, E.I. (2002). Spectroscopic studies of 1-aminocyclopropane-1-carboxylic acid oxidase: molecular mechanism and CO_2 activation in the biosynthesis of ethylene. J. Am. Chem. Soc. *124*, 4602–4609.
21. Zhang, Z.H., Ren, J.S., Stammers, D.K., Baldwin, J.E., Harlos, K., and Schofield, C.J. (2000). Structural origins of the selectivity of the trifunctional oxygenase clavaminic acid synthase. Nat. Struct. Biol. *7*, 127–133.
22. Zhang, Z.H., Ren, J.S., Harlos, K., McKinnon, C.H., Clifton, I.J., and Schofield, C.J. (2002). Crystal structure of a clavaminate synthase-Fe(II)-2-oxoglutarate-substrate-NO complex: evidence for metal centred rearrangements. FEBS Lett. *517*, 7–12.
23. Roach, P.L., Clifton, I.J., Hensgens, C.M., Shibata, N., Schofield, C.J., Hajdu, J., and Baldwin, J.E. (1997). Structure of isopenicillin N synthase complexed with substrate and the mechanism of penicillin formation. Nature *387*, 827–830.
24. Valegård, K., van Scheltinga, A.C., Lloyd, M.D., Hara, T., Ramaswamy, S., Perrakis, A., Thompson, A., Lee, H.J., Baldwin, J.E., Schofield, C.J., et al. (1998). Structure of a cephalosporin synthase. Nature *394*, 805–809.
25. Kadyrzhanova, D., Mccully, T.J., Warner, T., Vlachonasios, K., Wang, Z., and Dilley, D.R. (1999). Analysis of ACC oxidase activity by site-directed mutagenesis of conserved amino acid residues. In EU-TMR-Euroconference Symposium on Biology and Biotechnology of the Plant Hormone Ethylene II. (Dordrecht, Neth: Kluwer Academic Publishers), pp. 7–12.
26. Lay, V.J., Prescott, A.G., Thomas, P.G., and John, P. (1996).

Heterologous expression and site-directed mutagenesis of the 1-aminocyclopropane-1-carboxylate oxidase from kiwi fruit. Eur. J. Biochem. *242*, 228–234.

27. Wilmouth, R.C., Turnbull, J.J., Welford, R.W.D., Clifton, I.J., Prescott, A.G., and Schofield, C.J. (2002). Structure and mechanism of anthocyanidin synthase from Arabidopsis thaliana. Structure *10*, 93–103.
28. Valegård, K., van Scheltinga, A.C.T., Dubus, A., Ranghino, G., Öster, L.M., Hajdu, J., and Andersson, I. (2004). The structural basis of cephalosporin formation in a mononuclear ferrous enzyme. Nat. Struct. Mol. Biol. *11*, 95–101.
29. Turnbull, J.J., Nakajima, J., Welford, R.W.D., Yamazaki, M., Saito, K., and Schofield, C.J. (2004). Mechanistic studies on three 2-oxoglutarate-dependent oxygenases of flavonoid biosynthesis: Anthocyanidin synthase, flavonol synthase and flavanone 3-hydroxylase. J. Biol. Chem. *279*, 1206–1216.
30. Elkins, J.M., Ryle, M.J., Clifton, I.J., Dunning Hotopp, J.C., Lloyd, J.S., Burzlaff, N.I., Baldwin, J.E., Hausinger, R.P., and Roach, P.R. (2002). X-ray crystal structure of Escherichia coli taurine/α-ketoglutarate dioxygenase complexed to ferrous iron and substrates. Biochemistry *41*, 5185–5192.
31. Lloyd, M.D., Lee, H.J., Harlos, K., Zhang, Z.H., Baldwin, J.E., Schofield, C.J., Charnock, J.M., Garner, C.D., Hara, T., Terwisscha van Scheltinga, A.C., Valegård, K., et al. (1999). Studies on the active site of deacetoxycephalosporin C synthase. J. Mol. Biol. *287*, 943–960.
32. Myllyharju, J., and Kivirikko, K.I. (2001). Collagens and collagen-related diseases. Ann. Med. *33*, 7–21.
33. Lee, C., Kim, S.J., Jeong, D.G., Lee, S.M., and Ryu, S.E. (2003). Structure of human FIH-1 reveals a unique active site pocket and interaction sites for HIF-1 and von Hippel-Lindau. J. Biol. Chem. *278*, 7558–7563.
34. Elkins, J.M., Hewitson, K.S., McNeill, L.A., Seibel, J.F., Schlemminger, I., Pugh, C.W., Ratcliffe, P.J., and Schofield, C.J. (2003). Structure of factor-inhibiting hypoxia-inducible factor (HIF) reveals mechanism of oxidative modification of HIF-1 alpha. J. Biol. Chem. *278*, 1802–1806.
35. Dann, C.E., III, Bruick, R.K., and Deisenhofer, J. (2002). Structure of factor-inhibiting hypoxia-inducible factor 1: an asparaginyl hydroxylase involved in the hypoxic response pathway. Proc. Natl. Acad. Sci. USA *99*, 15351–15356.
36. Thrower, J.S., Blalock, R. III, and Klinman, J.P. (2001). Steady-state kinetics of substrate binding and iron release in tomato ACC oxidase. Biochemistry *40*, 9717–9724.
37. Brunhuber, N.M., Mort, J.L., Christoffersen, R.E., and Reich, N.O. (2000). Steady-state kinetic mechanism of recombinant avocado ACC oxidase: initial velocity and inhibitor studies. Biochemistry *39*, 10730–10738.
38. Que, L., Jr. (2000). One motif—many different reactions. Nat. Struct. Biol. *7*, 182–184.
39. Pereira-Netto, A.B. (2001). Effect of inhibitors of ethylene biosynthesis and signal transduction pathway on the mutiplication of in vitro-growth Hancornia speciosa. Plant Cell Tiss. Org. *66*, 1–7.
40. Zhang, Z.H., Barlow, J.N., Baldwin, J.E., and Schofield, C.J. (1997). Metal-catalyzed oxidation and mutagenesis studies on the iron(II) binding site of 1-aminocyclopropane-1-carboxylate oxidase. Biochemistry *36*, 15999–16007.
41. Liu, A., Raymond, Y.N.H., and Que, L., Jr. (2001). Alternative reactivity of an α-ketoglutarate-dependent iron(II) oxygenase: enzyme self-hydroxylation. J. Am. Chem. Soc. *123*, 5126–5127.
42. Ryle, M.J., Koehntop, K.D., Liu, A., Que, L., Jr., and Hausinger, R.P. (2003). Interconversion of two oxidized forms of taurine/α-ketoglutarate dioxygenase, a non-heme iron hydroxylase: evidence for bicarbonate binding. Proc. Natl. Acad. Sci. USA *100*, 3790–3795.
43. Henshaw, T.F., Feiga, M., and Hausinger, R.P. (2004). Aberrant activity of the DNA repair enzyme AlkB. J. Inorg. Biochem. *98*, 856–861.
44. Stadtman, E.R., and Levire, R.L. (2003). Free redical-mediated oxidation of free amino acids and amino acid residues in proteins. Amino Acids *25*, 207–218.
45. Hoffman, N.E., Yang, S.F., Ichihara, A., and Sakamura, S. (1982). Stereospecific conversion of 1-aminocyclopropanecarboxylic acid to ethylene by plant tissue. Plant Physiol. *70*, 195–199.
46. Pirrung, M.C., and Mcgeehan, G.M. (1986). Ethylene biosynthesis. 6. Synthesis and evaluation of methylaminocyclopropanecarboxylic acid. J. Org. Chem. *51*, 2103–2106.
47. Baldwin, J.E., Adlington, R.M., Lajoie, G.A., and Rawlings, B.J. (1985). On the biosynthesis of ethylene. Determination of the stereochemical course using modified substrates. J. Chem. Soc. Chem. Commun. 1496–1498.
48. Ryle, M.L., Liu, A., Muthukumaran, R.B., Ho, R.Y.N., Koehntop, K.D., McCracken, J., Que, L., Jr., and Hausinger, R.P. (2003). O_2- and α-ketoglutarate-dependent tyrosyl radical formation in TauD, an α-keto acid-dependent non-heme iron dioxygenase. Biochemistry *42*, 1854–1862.
49. Sharp, K.H., Mewies, M., Moody, P.C.E., and Raven, M.L. (2003). Crystal structure of the ascorbate peroxidase–ascorbate complex. Nat. Struct. Biol. *10*, 303–307.
50. Lamzin, V.S., Perrakis, A., and Wilson, K.S. (2001). The ARP/WARP Suite for Automated Construction and Refinement of Protein Models, Volume F (Dordrecht, The Netherlands: Kluwer Academic Publishers).
51. Jones, T.A., Zou, J.-Y., Cowan, S.W., and Kjeldgaard, M. (1991). Improved methods for the building of protein models in electron density maps and the location of errors in these models. Acta Crystallogr. A *47*, 11–119.
52. Brünger, A.T., Adam, P.D., Clore, G.M., DeLanno, W.L., Gros, P., Grosse-Kunstleve, R.W., Jiang, J.-S., Kuszewski, J., Nilges, M., Pannus, N.S., et al. (1998). Crystallography and NMR system: a new software suite for macromolecular structure determination. Acta Crystallogr. D Biol. Crystallogr. *54*, 905–921.